



# Universal and nonuniversal statistical properties of levels and intensities for chaotic Rydberg molecules

M. Lombardi, T. H. Seligman

## ► To cite this version:

M. Lombardi, T. H. Seligman. Universal and nonuniversal statistical properties of levels and intensities for chaotic Rydberg molecules. *Physical Review A : Atomic, molecular, and optical physics [1990-2015]*, 1993, 47, pp.3571-3586. 10.1103/PHYSREVA.47.3571 . hal-00974250

HAL Id: hal-00974250

<https://hal.science/hal-00974250>

Submitted on 5 Apr 2014

**HAL** is a multi-disciplinary open access archive for the deposit and dissemination of scientific research documents, whether they are published or not. The documents may come from teaching and research institutions in France or abroad, or from public or private research centers.

L'archive ouverte pluridisciplinaire **HAL**, est destinée au dépôt et à la diffusion de documents scientifiques de niveau recherche, publiés ou non, émanant des établissements d'enseignement et de recherche français ou étrangers, des laboratoires publics ou privés.

# Universal and nonuniversal statistical properties of levels and intensities for chaotic Rydberg molecules

M. Lombardi and T.H. Seligman\*

*Laboratoire de Spectrométrie Physique—Université Joseph Fourier de Grenoble, Boîte Postale No. 87,  
38402 Saint Martin d'Hères CEDEX, France*

(Received 23 September 1992)

We study Rydberg molecules taking into account the interaction between the rotational motion of the nuclei and the radial motion of the electron. This situation can be treated to a good approximation in quantum mechanics by the multichannel quantum-defect method which in turn has a well-defined classical limit. We are able to calculate very long sequences of levels and the corresponding amplitudes of wave packets. This allows us to study the statistical properties of both in detail. Our interest focuses on aspects of “quantum chaos” that can be particularly well understood in this case. Our main result is that, in a completely chaotic classical situation, where statistics of quantum-level spacings follow the expected universal Gaussian-orthogonal-ensemble behavior, and statistics of line intensities display the expected universal Porter-Thomas behavior, nonuniversal properties are explicitly contained in correlations between intensities and spacings, determined by the time needed for the classical system to mix on a length scale given by the quantum wavelength.

PACS number(s): 03.65.Sq, 33.90.+h, 24.60.Lz, 05.45.+b

## I. INTRODUCTION

Interest in the effects of classical chaos in molecular systems has increased enormously in recent years [1–9]. Both theoretical studies and analyses of experiments are increasingly popular and successful. Yet extensive calculations have been limited to simple and, with the exception of the hydrogen atom in a magnetic field [10], unrealistic systems such as billiards [11, 12] and anharmonic oscillators [13, 14, 12].

Recently it has been suggested [5] that Rydberg molecules may provide an excellent test ground for many of our ideas. Simplifying to the most basic case these molecules can be viewed as a rotating system with positive charge and cylindrical symmetry that binds one electron in an orbit that is at large distances hydrogenic. At short distances the orbit is principally distorted by the quadrupole moment of the rotor and this causes a coupling between the rotational motion of the nuclei and the electronic motion. The quantum problem can be solved with high accuracy for large numbers of levels using the quantum-defect method [15]. Furthermore, the approximation itself has a classical limit that can be readily simulated on a computer [5]. When the periods of the electron are multiples of the period of rotation of the core we have a resonance and the system is nearly integrable except for very large couplings; off resonance the system is almost entirely chaotic for very moderate coupling. We thus have a system that is realistic, accessible to easy numerical treatment, and that displays a transition from near integrable to very chaotic situations.

In this paper we shall proceed to investigate this system off resonance in a fully chaotic situation in order to study not only the spectra as is done most commonly, but also the intensities of wave packets of physical interest. A natural basis to do this is suggested by the experimental situation and the calculation technique employed.

Indeed it is possible to deposit wave packets on well-defined points of the sphere that determines the position of the angular momentum of the electron with respect to a molecular reference frame defined by the axis and the angular momentum of the core, and also to compute projections of the Wigner function on this space.

In order to do this we shall briefly describe the physical situation and the approximations we use following the lines of Ref. [5]. Next we proceed to show the results of actual calculations both in classical and quantum mechanics for an angular momentum of  $L = 40$  for the core and a total angular momentum of  $J = 200$ . These numbers were chosen in order to obtain long sequences of states that display independent statistics without incurring prohibitive computing cost or time. Next we proceed to analyze the results both for the energy spectrum and for the amplitudes. We use first of all the conventional tools of spectral analysis such as Fourier transforms [3], nearest-neighbor spacing distributions,  $\Delta_3$  and  $\Sigma^2$  statistics [16].

We then proceed in Sec. IV to the main subject of this paper, namely the analysis of “real” spectra with their corresponding intensities, i.e., of spectra associated with wave packets. This is important for two reasons: first, with conventional spectral analysis we throw away important information that is actually contained in typical experimental spectra; second, it is not always possible to extract an energy (stick) spectrum from the data.

Note with respect to this last point that, for example, in nuclear physics the question of missing levels due to weak intensities or overlaps severely limits the experimentally available energy spectra as extracted, say, from neutron absorption data. In molecular physics the problem resides often with the impossibility to resolve lines experimentally, except for triatomics, but even in this case weak intensities will certainly also cause difficulties [9]. With respect to the first point the shortest (unsta-

ble) periodic orbits show up more markedly in Fourier transforms obtained from intensity spectra than from energy spectra, because the average area of the latter tend generically to zero for zero time in a fully chaotic system [17]. Furthermore, they carry an important nonuniversal information: the time, related to Lyapunov exponents, for the chaotic system to attain the mixing situation on a length scale defined by the quantum wavelength. We show explicitly that this information is contained neither in the level-spacing statistics nor in the amplitude or line-intensity statistics, but in the correlations between them.

To analyze the data we apply a Fourier analysis [3] to recover short-time information but consider also other possibilities to display energy-amplitude correlations. A straightforward generalization of the number variance  $\Sigma^2$  to an intensity variance proves useful and handy.

Finally we shall conclude by discussing the difficulties as well as the opportunities that lie in the path of statistical interpretation of chaos in terms of spectra, as displayed by this example. Also we shall briefly mention which features have been observed experimentally and what might have to be done to confirm our other findings.

## II. RYDBERG MOLECULES AND THE QUANTUM-DEFECT METHOD

The principle of the phenomena is best seen on the classical model which has been shown to be the classical limit of the quantum-mechanical approximation that follows [5]. When the outer electron is far from the molecular core (i.e., most of the time for a Rydberg electron), it senses only the central Coulomb field  $-1/r$  of the core [charge = 1; we will use throughout atomic units (a.u.):  $e = \hbar = m = 1$ ]. Its orbit is hydrogenic and its angular momentum  $\mathbf{L}$  is fixed in the laboratory frame. Meanwhile the core rotates freely around its angular momentum  $\mathbf{N}^+$ , which is also fixed in the laboratory frame, at an angular velocity  $\omega_N = N^+/I = 2\pi/T_N$  (where  $I$  is its moment of inertia related to the rotational constant according to standard molecular spectroscopic notation [18] by  $B = 1/I$ ). These two fixed angular momenta  $\mathbf{L}$  and  $\mathbf{N}^+$  add up to  $\mathbf{J}$  which is also fixed in the laboratory frame. In the molecular core frame the  $z$  axis is chosen along the core axis and the  $x$  axis along the vector  $\mathbf{N}^+$  (Fig. 1), which is perpendicular to the core axis if the intrinsic (electronic) angular momentum of the core is zero as is the case in all our explicit calculations. The electronic angular momentum  $\mathbf{L}$  seems to rotate in the opposite direction around the body fixed  $x$  axis  $OX$ . During the collision the electron feels the cylindrically symmetric part of the potential of the core. Due to this cylindrical symmetry the projection of  $\mathbf{L}$  on the core axis  $\Lambda_L = L \cos \theta_e$  remains constant during the collision. The collision can then be described, within the approximations discussed in [5] and below, by a  $\theta_e$ -dependant rotation of  $\mathbf{L}$  around  $OZ$ . The simplest form compatible with symmetry restrictions is

$$\delta\phi_e = K \cos \theta_e, \quad (2.1)$$

where  $K$  is a coupling constant. The conservation of total

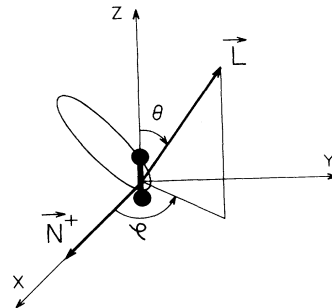


FIG. 1. Molecular reference frame.  $\mathbf{N}^+$  is the angular momentum of the ionic core,  $(\theta_e, \phi_e)$  are the polar angles of the angular momentum  $\mathbf{L}$  of the Rydberg electron with respect to  $OZ$ .

angular momentum  $\mathbf{J}$  implies that the molecule experiences a simultaneous recoil which changes both the direction and magnitude of  $\mathbf{N}^+$ . This implies an exchange of energy between the electron and core (keeping the total energy  $E$  constant).

The motion of the Rydberg electron's angular momentum  $\mathbf{L}$  (supposed of constant magnitude as discussed below) can thus be described as two consecutive steps: (i) when the electron is far away a rotation around the  $OX$  axis at constant speed  $-\omega_N$  during the time  $T_e$  (period of the electron orbit), and (ii) during the collision a rotation along the  $OZ$  axis by an angle  $\delta\phi_e$  given by Eq. (2.1), and a simultaneous recoil of molecular frame due to the conservation of  $J$ . It is the competition between these two motions which leads to chaos [5].

Notice that a resonance appears when  $T_e$  is a multiple of  $T_N/2$ . In this case, when the electron returns it sees the core in the same position at which it left it. Then, as was shown in Ref. [15], the Born-Oppenheimer approximation holds again,  $\Lambda_L$  is an approximate constant of motion for the whole process (not only during the collision), and thus the motion is anew approximately regular. This produces the experimentally observed "stroboscopic fringes" in the spectra [15] which prompted all further study on this subject.

Finally notice the close analogy of this system with the "kicked spin" [19]. It can be shown that the kicked spin is the limit of the present system when  $L \ll J$ , so that one can neglect recoil and exchange of energy effects. We nevertheless kept the Rydberg model both because it is experimentally more realistic and because it allows more flexibility of the results.

Quantum mechanically, the computation of a Rydberg molecular spectrum using the multichannel quantum-defect theory (MQDT) proceeds schematically as follows (for details and proofs refer to the original papers [20, 15]). According to the distance  $r$  between the outermost (Rydberg) electron and the remaining molecular core, configuration space is divided into two parts: a collision region ( $r < r_0$ ) and an asymptotic region ( $r > r_0$ ).  $r_0$  is of the order of the core size, and is chosen so that in the asymptotic region the electrostatic potential felt by the outer electron can be considered as spherically symmetric Coulomb potential  $1/r$  (with charge=1), whereas in the

collision region the whole potential produced by the core (which includes spherically and cylindrically symmetric parts) is important.

In the asymptotic region, the molecular axis is immaterial for the outer electron, which is thus quantized in the laboratory frame, with a wave function  $f(r)Y_L^M(\theta_e, \phi_e)$ . The core is a free symmetric top, with a wave function

$$|iN^+\Lambda^+M_{N^+}\rangle = \Psi_i^{\Lambda^+} R_{M_{N^+}\Lambda^+}^{N^+*}(\phi_c, \theta_c, 0), \quad (2.2)$$

where  $\Psi_i^{\Lambda^+}$  is the internal wave function of the symmetric core, including its electronic degrees of freedom as well as possible vibrations of the nuclei.  $\Lambda^+$  indicates the internal angular momentum of the core and by consequence also the projection of the total angular momentum of the core  $N^+$  on the axis of the top, which in our calculations we shall choose equal to zero.  $\theta_c, \phi_c$  are polar angles of the core axis,  $R$  is a rotation matrix as defined by Messiah [21], and  $M_{N^+}$  is the projection of  $N^+$  on the  $z$  axis of the laboratory frame. The wave function of the whole molecule [Hund's case (d) [18]] is then obtained by coupling  $L$  and  $N^+$  by a standard Clebsch-Gordan coefficient

$$\begin{aligned} & |iN^+\Lambda^+LJM_J\rangle \\ &= \sum_{M,M_{N^+}} \langle L, N^+ MM_{N^+} | L, N^+ JM_J \rangle \\ &\quad \times f(r)Y_L^M(\theta_e, \phi_e) |iN^+\Lambda^+M_{N^+}\rangle. \end{aligned} \quad (2.3)$$

In this region the total energy  $E$  can be written as

$$E = \frac{-\mathcal{R}}{\nu_{N^+}^2} + E^+ + BN^+(N^+ + 1), \quad (2.4)$$

where  $E^+$  is the electronic plus vibrational energy of the core (taken as energy zero in the foregoing) and  $\mathcal{R}$  the Rydberg energy (0.5 a.u.). This formula defines the  $N^+$ -dependent principal quantum number  $\nu_{N^+}$ —which now needs not be an integer—of the outer electron as a function of energy.

In the collision region to the contrary the outer electron feels the cylindrically symmetric part of the core and the Born-Oppenheimer approximation is valid. The wave function [Hund's case (a) or (b) (if the total electronic spin is zero as supposed in the foregoing)] [18] is given by

$$|i\Lambda^+\Lambda^+LJM_J\rangle = \Psi_{i,L,\Lambda^+}^{\Lambda} R_{M_J,\Lambda}^{J*}(\phi_c, \theta_c, 0), \quad (2.5)$$

where  $\Psi_{i,L,\Lambda^+}^{\Lambda}$  now includes both the core and the outer electron coordinates in the molecular frame,  $J$  is the total angular momentum,  $M_J$  its projection on the laboratory frame  $z$  axis, and  $\Lambda$  its projection on the top axis.

Writing the labels  $\Lambda^+$  and  $L$  for the function  $\Psi$  implies two subsidiary approximations: The electronic states of the core are not coupled by the interaction with the outer electron, so that  $\Lambda^+$  remains a good quantum number, and the different  $L$  states of the outer electron, which are split by the quantum defects produced by the spherically symmetric non- $1/r$  Coulomb part of the core potential, are not significantly mixed by the only cylindrically

symmetric part of the same potential. The first approximation is very good, the second is more questionable and must be corrected for in detailed molecular computations [15], but it is good enough to be maintained in the present analysis where not supposing it would introduce severe technical complications (increase in dimensionality) irrelevant for our purpose.

The two preceding wave functions must then be connected at  $r = r_0$ . This connection contains two parts [15].

(i) An angular part: a change of reference frame from molecular to laboratory for the outer electron which entails an angular recoupling matrix  $U$  that actually reduces to a simple Clebsch-Gordan coefficient in this case:

$$U_{\Lambda_L,N^+}(J, L, \Lambda^+) = \langle (L, J)N^+ - \Lambda^+ | (L, J)\Lambda_L - \Lambda \rangle. \quad (2.6)$$

(ii) A radial part. The radial wave function  $f$  of the outer electron is in general the sum of two Coulomb functions, one rising and the second decreasing exponentially for  $r \rightarrow \infty$ . Demanding the continuity of the wave function at  $r = r_0$  in the molecular frame between the inner (Born-Oppenheimer) wave functions labeled by  $\Lambda$  and the outer wave function entails a dephasing  $\pi\mu_\Lambda$  of the outer-electron Coulomb functions with respect to the value they would have in a pure Coulomb potential. For positive energies  $E$ , when the outer electron can go to infinity, these phase shifts are identical with collision phase shifts. For bound states, demanding that wave functions go to zero at infinity, i.e., that the coefficient of the rising Coulomb function be zero, leads to the fundamental set of equations

$$\sum_{\Lambda_L=-L}^L U_{\Lambda_L,N^+} \sin[\pi(\nu_{N^+} + \mu_\Lambda)] A_\Lambda = 0 \quad (N^+ = J - L, \dots, J + L), \quad (2.7)$$

where the  $A_\Lambda$  are to be determined by these equations. All the coefficients of this set of equations depend on the energy  $E$ , mainly through the energy dependence of the  $\nu_{N^+}$  implied by Eq. (2.4). There is also an energy dependence of the phase shifts  $\mu_\Lambda$  as in collision theory. The latter is usually weak for high Rydberg states because the energy of the outer electron accelerated by the core from nearly zero velocity at large distance to its value at  $r = r_0$  is hardly modified by the small changes in energy between states accumulating below the ionization limit. The energy dependence of the  $\mu_\Lambda$  will thus henceforth be neglected. This set of equations has nontrivial solutions only when its determinant is zero, which gives the quantization rules for energy. The resulting  $A_\Lambda$  are the coefficients of the outer-electron wave function when expressed in the Born-Oppenheimer basis.

The key point with respect to chaos of this system is that  $N^+$  is a good quantum number in the asymptotic wave functions (2.3), whereas  $\Lambda$  is a good quantum number for Born-Oppenheimer wave functions (2.5). For generic values of the couplings (i.e., the phase shifts  $\mu_\Lambda$ ) the actual wave function is an  $r$ -dependent mixture of

the two. Neither  $N^+$  nor  $\Lambda$  is a good quantum number. One recovers the asymptotic wave functions only for zero coupling. The Born-Oppenheimer wave function on the other hand is not only a reasonable approximation at low energy (strong binding) but also when the resonance condition is fulfilled. Quantum mechanically this is the case when an integer multiple of the energy difference between consecutive Rydberg states  $-\mathcal{R}/n^2$  is equal to twice (for symmetry reasons) the energy difference between consecutive rotator states  $BN^+(N^+ + 1)$ .

The connection between the classical and the quantum case is established by the relation

$$\mu_\Lambda = \mu_0 - \frac{K}{4\pi L} \Lambda_L^2 \quad (2.8)$$

between the classical coupling constant  $K$  and the quantum phase shifts  $\mu_\Lambda$ .

### III. CLASSICAL AND QUANTUM-MECHANICAL RESULTS

In this section we shall apply the models and methods discussed in the previous section to perform a specific calculation and display the results. We shall choose a core intrinsic momentum  $\Lambda^+ = 0$  (so that  $\Lambda_L = \Lambda$  and we drop the subscript  $L$  in what follows), a core angular momentum  $L = 40$ , a total angular momentum  $J = 200$ , and a rotation constant  $2B = 2.5 \times 10^{-12}$  which gives a first resonance  $T_e/T_N = 0.5$  for  $\nu_{200} = 1004$ . Since we want to study in this paper a fully chaotic situation we choose the interval  $\nu_{200} = 877.5 \pm 25.0$ , centered on the nonresonant value  $T_e/T_N = 0.331$ . Here we specify the energy range by the value of  $\nu_{N^+} = \nu_{200}$  [related to energy by Eq. (2.4)] because 200 is the average value of  $N^+$  which ranges in the interval  $J - L \leq N^+ \leq J + L$ . Thus we actually have  $2L + 1 = 81$  states for each value of  $\nu_{200}$ . They are split into two (Krönig [18]) symmetry classes according to the relation

$$|\Lambda\pm\rangle = (|+\Lambda\rangle \pm |-\Lambda\rangle)/\sqrt{2}. \quad (3.1)$$

The coupling constant  $K \approx -12.5$  was chosen reasonably large and according to Eq. (2.8) corresponds to a maximum quantum defect  $\mu_{40} = 39.8765$  (we avoided an integer value for fear that integer phase shifts had peculiar properties in quantum mechanics). We have also made computations with a small  $K = -1.25$  in the resonance region contained in the interval  $\nu_{200} = 1004 \pm 25$ , which gives a nearly regular situation. These last computations will be described in detail in a future paper, but we shall show some results in the present paper, when they are useful for the sake of comparison. Occasionally, when pictures are more clear due to the smaller number of levels, we display in what follows results for  $L = 10$ ,  $J = 50$ ,  $2B = 6.4 \times 10^{-10}$ , with the same values of  $T_e/T_N$  and of  $K$ , which correspond to the same classical limit with  $\hbar$  divided by 4.

Figure 2 shows the Poincaré section for classical motion at the center of the interval for the chaotic situation. The Poincaré surface of section here is simply a unit sphere,

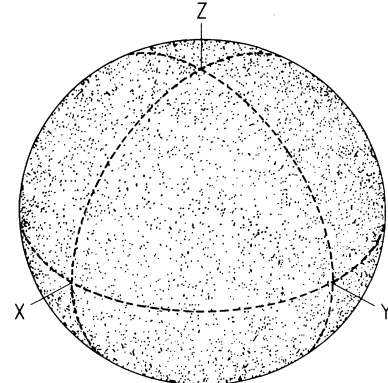


FIG. 2. Poincaré surface of section in the chaotic case. The section is here the sphere which represents the direction with respect to the molecular reference frame of the angular momentum of the electron  $\mathbf{L}$  immediately after every collision with the core.

each point indicating the direction of the electron angular momentum  $L$  after every collision. It clearly displays the fact that we are indeed in a fully chaotic situation. Poincaré sections in integrable cases have been shown in Ref. [5].

Next we used the quantum-defect method to obtain spectra in both intervals. In the chaotic area we met no particular problems, and were able to obtain nearly 2000 levels as well as the projections  $A_\Lambda$  of the corresponding eigenfunctions in about 20 h on an advanced personal computer. For the other interval, when on resonance, we were able to obtain the eigenvalues in the same way, but the amplitudes became in certain cases totally unreliable. Two hours of computation with 128 bits on a CDC990 computer in vector mode were necessary to obtain equivalent results. Note that this highlights an important problem: for the near-integrable system there is no level repulsion so that we find very close levels. This, in contrast with the strong level repulsion expected for chaotic systems, leads us to very inaccurate eigenfunctions, because the computed wave function evolves from a given function to a nearly orthogonal function in a very narrow energy interval. This problem is accentuated in this method as the orthogonality of successive eigenvectors is not assured by the method itself, because we compute only projections in  $\Lambda$  space, whereas orthogonality is required for the total eigenfunction. We thus have to be very careful in judging the correctness of the intensities we find. Yet after taking the corresponding precautions we have reliable results.

The eigenvalues for a case  $L=10$ ,  $J=100$  have been shown in Figs. 9(c) and 9(d) of Ref. [5] on and off resonance for just about 20 levels near the center of the interval. By direct inspection we note that the spectra in both cases nearly repeat after 11 levels. Over larger distances this correlation is slowly destroyed. This is one difference of the present system with the kicked spin which would give a perfectly periodic spectrum. This evolution of the spectrum is thus a consequence of taking into account the recoil of the molecular frame after each collision due to the conservation of total angular momentum. The

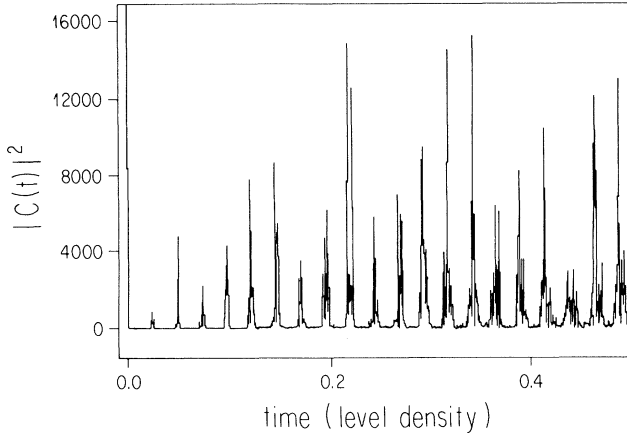


FIG. 3. Fourier transform of the “stick” (energy) spectrum in the chaotic case  $L = 40$ , symmetry +,  $J = 200$ ,  $2B = 2.5 \times 10^{-12}$ ,  $K = -12.5$ ,  $\nu_{200} = 877.5 \pm 25.0$ , centered on  $T_e/T_N = 0.331$ .

square of the modulus of the Fourier transform (FT) of the spectrum of eigenvalues off resonance for the present case  $L=40$ ,  $J=200$  symmetry + is shown in Fig. 3. The near periodicity of the spectrum gives the global picket-fence aspect of this FT, with a time spacing equal to the near-constant classical period, or also equal to  $1/41$  in reduced units of time equals to  $\hbar\rho$ , where  $\rho$  is the level density. The recoil effect, which makes the period change slightly after each collision, makes the width of these peaks increase in time. Equivalently one can say than in the energy interval  $\nu_{200} = 877.5 \pm 25$ , which is Fourier transformed, there is a narrow range of classical periods. This range is relatively small because the conservation of total angular momentum  $J$  makes the core angular momentum  $N^+$  vary only slightly between  $J-L = 160$  and  $J+L = 240$ , which entails a small variation of core energy and thus of  $\nu_{N^+}$  and the electronic period  $T_e$  according to Eq. (2.4). Each peak has a very noisy structure which is a wave interference effect analog to the laser “speckle” phenomenon [3]. When going nearer to the classical limit the structure remains equally noisy (100% noise modulation), but the number of noise spikes contained within a given classical peak increases as  $1/\hbar$ , which enables us to recover the classical smooth result with increasing accuracy by averaging over the spikes. It is important to notice that this is *not* a structure associated with multiple periodic orbits present in the classical system [22]. We have computed the periodic orbits in our case: when the energy varies in the interval defined by  $\nu_{200} = 877.5 \pm 25.0$  on which spectra are Fourier transformed, there are four periodic orbits bunched in the first peak, 54 to 62 periodic orbits bunched in the second peak, 154 to 310 periodic orbits bunched in the third peak, etc. Note that the numbers for the second and third peak change over that interval. To resolve the structure associated with these individual periodic orbits we would have to go much deeper in the semiclassical approximation. Instead we prefer to think of a practical way to extract useful information from such essentially unresolved peaks.

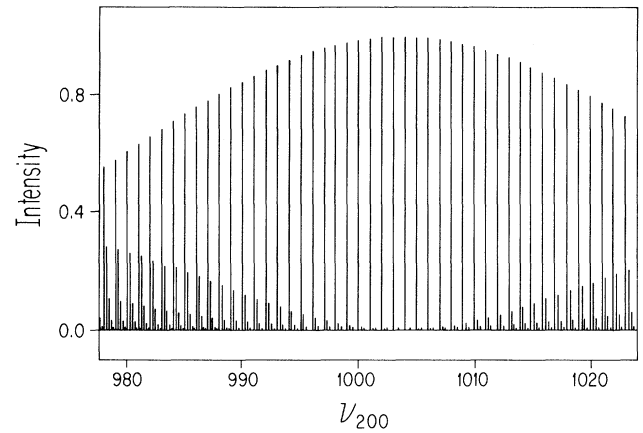


FIG. 4. True, intensity-weighted, spectrum for  $\Lambda = L$ , symmetry + excitation in the resonant (regular) case  $L = 40$ ,  $J = 200$ ,  $2B = 2.5 \times 10^{-12}$ ,  $K = -1.25$ ,  $\nu_{200} = 1004 \pm 25$ , centered on  $T_e/T_N = 0.5$ . “Stroboscopic effect” [15]: nearly only one eigenstate in every period of 41 is excited at the center of the resonance.

We now proceed to discuss intensities of wave packets projected on the spaces with fixed values of  $\Lambda$ . Figure 4 shows a typical on-resonance case, where the packet was deposited on the rotor axis ( $\Lambda = 40$ ); we see that near the center of the interval this packet excites essentially a single eigenstate, while toward the edges there is an onset of mixing between the eigenstates. This is the “stroboscopic effect” [15]. On resonance we may see much more mixing if the wave packet is chosen to cover parts of significantly different invariant tori, but this is of no particular interest in the present paper. In Fig. 5 we show an intensity spectrum for a packet located at  $\Lambda = 10$  for the above-mentioned case  $L = 10$ ,  $J = 50$ , in the chaotic situation.

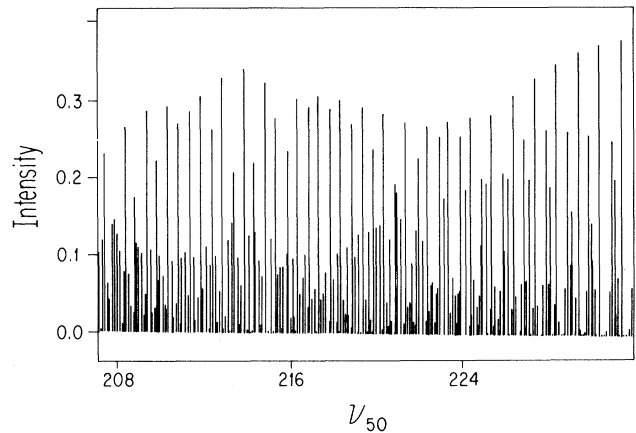


FIG. 5. True, intensity-weighted, spectrum for  $\Lambda = +L$ , desymmetrized [see Eq. (3.1)] excitation in the nonresonant (chaotic) case  $L = 10$ ,  $J = 50$ ,  $2B = 6.4 \times 10^{-10}$ ,  $K = -12.5$ ,  $\nu_{50} = 219.5 \pm 12.5$ , centered on  $T_e/T_N = 0.331$ . With respect to Fig. 4, notice that all eigenstates are excited in a complex and rapidly energy varying manner, but that it is possible to follow by eye intensity regularities which point to intensity-spacings correlations.

The near periodic features are conserved but vary more strongly with energy and we suspect correlations between intensities and level positions which enable us to follow by eye regularities in amplitudes.

An important question that arises in this context relates to the degree in which we find ourselves in the classical limit. We have to remember that this limit is reached for Coulomb problems near threshold. But we really have to go one step further to gain a clear insight. We have to see whether the behavior of classical density packets is followed closely by the Wigner function or some similar quantum objects. We prefer the Wigner function because of its clear physical meaning as the density operator in the phase-space description of quantum mechanics [23]. To illustrate this point we show in Figs. 6(a)–6(c) the classical evolution of a ring on the Poincaré section after zero, one, or two revolutions of the electron. For clarity of the picture we use again the  $L = 10$ ,  $J = 50$ , and  $K = -12.5$  case. This situation is actually further from the classical limit, but in the quantum case the number of projections is much smaller and thus the picture clearer. Figures 7(a)–7(c) show the corresponding Wigner functions, and we see clearly that they follow the classical behavior quite closely. Similarly, packets deposited on

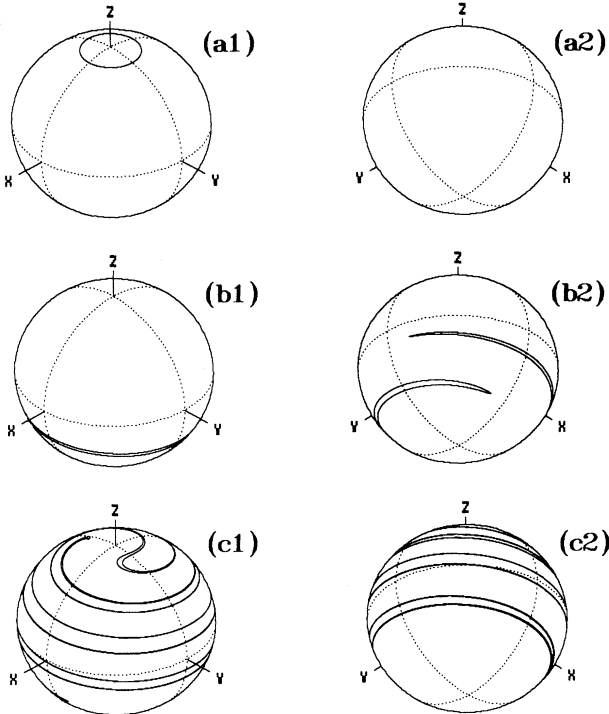


FIG. 6. Time evolution of a ring on the Poincaré surface of section in the nonresonant (chaotic) case  $L = 10$ ,  $J = 50$ ,  $2B = 6.4 \times 10^{-10}$ ,  $K = -12.5$ ,  $T_e/T_N = 0.331$  in the  $YOZ$  plane. Start: (a1) front view, (a2) rear view; after 1 collision: (b1) front view, (b2) rear view; after 2 collisions: (c1) front view, (c2) rear view. The ring is first rotated without deformation around the  $OX$  axis by 0.331 turns, then is stretched around the  $OZ$  axis by a  $-12.5 \cos(\theta_e)$  pseudorotation [see Eq. (2.1)]. Notice the “baker’s transformation” leading to mixing.

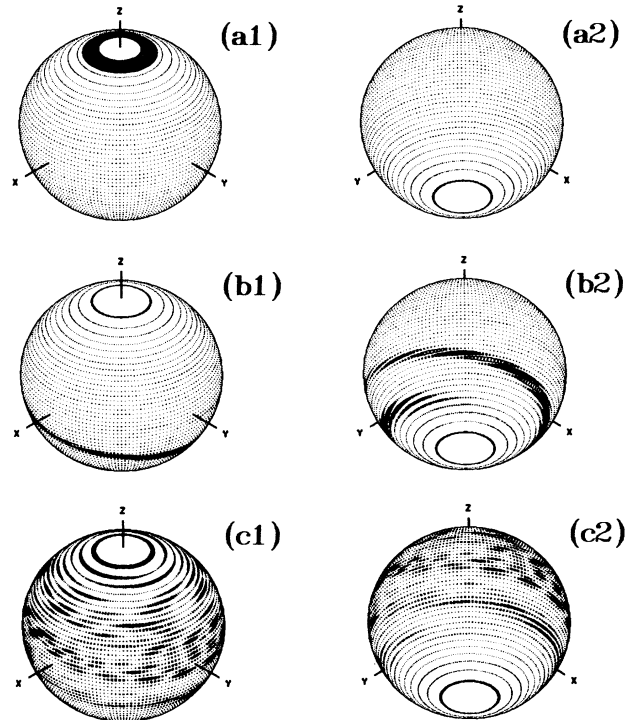


FIG. 7. Time evolution of the Wigner function for a  $\Lambda = +L$ , desymmetrized [see Eq. (3.1)] initial state with the same parameters as in Fig. 6. Filled box: positive value; empty box: negative value of the Wigner function. Notice the close similarity with the classical Poincaré section, showing that we are deep in the semiclassical limit.

other points of the Poincaré section display the expected behavior.

We may thus say that we are quite deep in the semiclassical region and any behavior that deviates from the expected results for chaotic or integrable systems will be meaningful. This is not to imply that deviations prove semi-classical results to be wrong. A well-known example shows that the limiting behavior may be reached only for very large quantum numbers [24]. On the other hand, persistent deviations must be considered in any analysis of data and if they occur in a physical system they contain important information about this system.

#### IV. LEVEL STATISTICS

In order to analyze fluctuations of a spectrum we first have to unfold the spectrum to obtain a constant density. In the present case we completed this task by simply considering the variable  $\nu_{200}$  similar to the action of the hydrogenic orbitals, instead of the energy. The coupling to the rotational states introduces no significant density variation over the energy range of interest. We can thus directly apply any statistical tests we have in mind to the spectra we obtained in the previous section.

We shall start by looking at the Fourier transform smoothed over intervals corresponding to one typical period. The reason for this smoothing is that it will yield

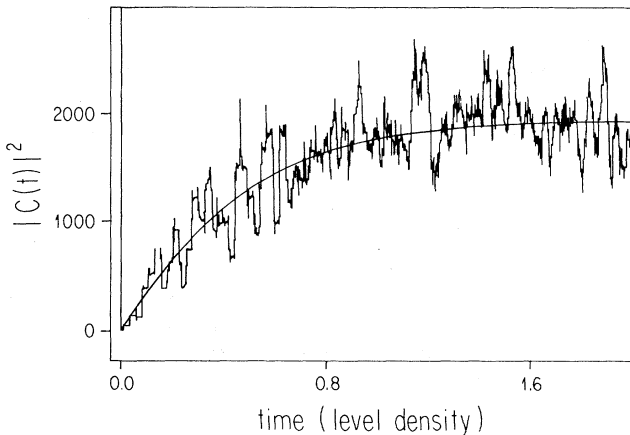


FIG. 8. Smoothing of the Fourier transform shown in Fig. 3 of a chaotic stick (energy) spectrum. Each point is the square smoothing between times  $t - T_e/2$  and  $t + T_e/2$ . Superimposed is the theoretical curve corresponding to the GOE (no adjustable parameter).

the area under the Fourier transform, averaged over the “speckle noise” mentioned in Sec. III. This area is the relevant quantity in statistical theory of spectra: the speckle noise obtained when Fourier transforming a single long spectrum is of course not truly a noise, but carries the information about the individual line positions in the spectrum, which is averaged upon in a statistical theory (see Refs. [3, 9] and Appendix A).

This transform is shown in Fig. 8 off resonance. The corresponding unsmoothed Fourier transform was shown in Fig. 3. The smoothed FT display the “correlation hole” [3] expected when the classical system is chaotic, so that level spacings follow Gaussian-orthogonal-ensemble (GOE) statistics [17, 3]. Notice that the universal GOE law, which predicts that the FT should go linearly to zero when time goes to zero is obeyed down to the first peak. This means that nonuniversal shortest periodic orbits, invoked to explain non-universal properties in, e.g., the zeros of the Riemann’s  $\zeta$  function [25], do not show up in our case, at least when averaged over the four periodic

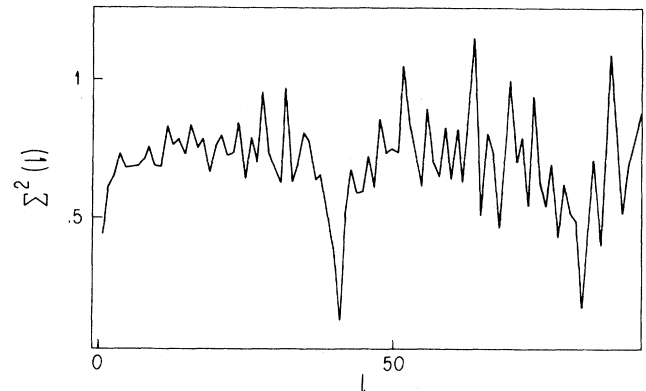


FIG. 10.  $\Sigma^2(l)$  number variance at large  $l$  for  $L = 40$ , symmetry  $+$ ,  $J = 200$ , in the chaotic case. Notice the 41 periodicity of the curve. Since the spectrum repeats itself nearly identically after a period of 41, the number variance is nearly equal to zero at  $l$  multiples of 41.

orbits bunched in the first peak. This situation forbids the possibility to use the amplitude of individual periodic orbits to measure on the energy spectra the nonuniversal Liapunov exponents [22]. Thus the only usable information which remains in the spectrum is its universal average GOE behavior, plus the nonuniversal bunching at multiples of the electron period. A remnant of the line-by-line information, however, is the “noise” which makes the smoothed FT of Fig. 8 differ from the theoretical smooth GOE curve. While this noise may carry some information about nonuniversal properties, we know no sensible way to extract it.

Looking now to more conventional measures of statistical properties of spectra, it was shown in Ref. [5] that the  $\Delta_3$  statistic displays a pronounced saturation “kink” [13], but apparently none of the more interesting features of the spectrum associated with the periodicity. We shall, therefore, remember the relevant remark of Verbaarschot [26], who pointed out that  $\Delta_3$  omits important information contained in the two-point function and in the number variance  $\Sigma^2$ . Indeed if we plot the short-range part of  $\Sigma^2$  both on and off resonance (Fig. 9), we see essentially the expected behavior for near-integrable and near-chaotic situations. On the other hand, we see fairly periodic structures with clear periodicity 41 over longer distances in Fig. 10. Notice then similar looking features were observed in regular systems [27] or in mixed systems [28] (associated with stable periodic orbits), but that this is new for a fully chaotic system. At any rate one sees readily that there is much more involved than the standard long-range stiffness.

We shall not discuss the implications of our results at this point, but rather in the next section present the phenomenology we found for intensity spectra in order to discuss both together in Secs. VI and VII.

## V. STATISTICS OF INTENSITY SPECTRA

The statistical analysis of wave functions is a very difficult problem because of the basis dependence of any rep-

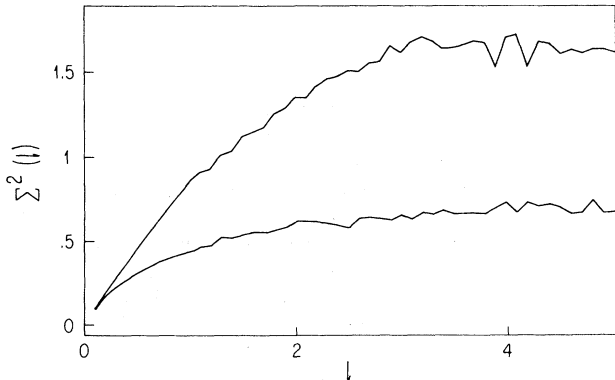


FIG. 9.  $\Sigma^2(l)$  number variance at small  $l$  for  $L = 40$ , symmetry  $+$ ,  $J = 200$ , for the regular (top) and chaotic (bottom) cases.

resentation of a function. As we pointed out elsewhere we need some guidelines to choose the basis in which we are interested because the orthogonal invariance implicit in an arbitrary choice is destroying possible signatures and simulates chaos [30].

In the present system we are in a fortunate situation. Our method provides us with a projection of the eigenfunctions on the space of angular-momentum projections  $\Lambda$ , i.e., a low-dimensional space that has physical significance throughout the energy range of interest. Actually it corresponds to wave packets we may form with adequate laser excitations [15]. By consequence corresponding intensities are also accessible to experiment. We thus have a basis of wave packets which we can shift at our wish in energy, i.e., exactly what is best suited for an analysis of functions [30]. The fact that we deal with a projection rather than with a complete function turns out to be more of an advantage than a disadvantage, and we are thus not obliged to reconstruct the full function.

We shall start by looking at Fourier transforms of off-resonance spectra. In this case we take the intensities  $I(i)$  of level  $i$  for a wave packet with given  $\Lambda$  and perform the transformation and smoothing over the characteristic electronic period. We show in Fig. 11 the result for the value  $\Lambda = 40$  which displays most clearly the phenomenon we want to discuss.

In order to discuss this figure we have to determine the reference we expect for a chaotic system. If indeed the energy spectrum is of GOE type and the intensities are independent of the levels and have a Porter-Thomas [29] distribution as expected for a GOE, then we expect the correlation hole seen in the energy spectrum to be filled

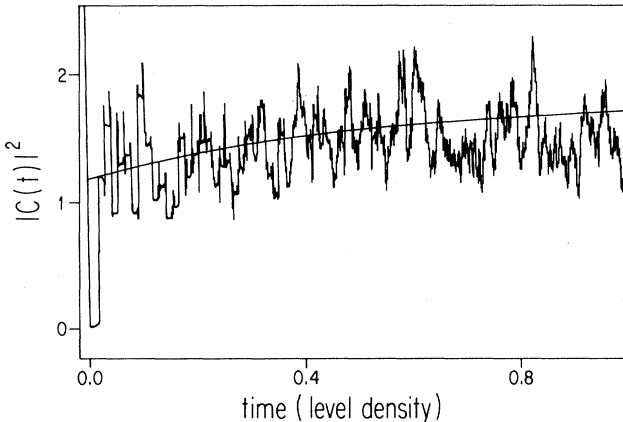


FIG. 11. Smoothed Fourier transform for an intensity-weighted spectrum for a  $\Lambda = +L$ , desymmetrized [see Eq. (3.1)] excitation (corresponding to the same classical limit as Fig. 6), in the chaotic case  $L = 40$ ,  $J = 200$ ,  $2B = 2.5 \times 10^{-12}$ ,  $K = -12.5$ ,  $\nu_{200} = 877.5 \pm 25.0$ , centered on  $T_e/T_N = 0.331$ . The smooth curve is the reduced correlation hole expected if intensities and spacings are independent. There is no adjustable parameter:  $N$  and  $\langle I \rangle$  in Eq. (A8) are taken from data,  $b_2$  corresponds to GOE, and  $\langle I \rangle^2/\langle I^2 \rangle = 1/3$  according to Porter-Thomas statistics. The width of the hole immediately after the origin is significantly  $\frac{3}{2} T_e$ , indicating a zero value of  $|C(t)|^2$  after one revolution. Only for later times does the “experimental” curve oscillate around the expected curve.

by two thirds, i.e., a hole of  $1/3$  remains as we show in Appendix A.

In addition to a global behavior which may correspond to what is expected, with a lot of statistical noise (due to the fact that noise corresponds basically to an average over 41 levels, i.e., with a relative  $1\sigma$  deviation of  $1/6.5$  as shown in Sec. VI), we see that the area of the first peak at time  $T_e$  is zero, and only for later times the results begin to oscillate around the expected curve. This could be due to two effects: either the distribution of intensities deviates in a sensitive way from the expected one or there exists a correlation between energies and intensities. To check the first hypothesis we plot in Fig. 12 a histogram of the amplitudes, which should be Gaussian if the intensities are Porter-Thomas distributed. Clearly the expected rule is satisfied so that the first hypothesis is not valid. But an ocular inspection of the intensity spectrum in Fig. 5 suggests the second hypothesis and therefore we perform the following test. We take the intensities shown in Fig. 5 and shuffle them randomly over the entire spectrum without changing the positions of the peaks, i.e., the energies as shown in Fig. 13: in these two figures we have displayed for clarity the  $L = 10$ ,  $J = 50$  case. On this spectrum we again perform a Fourier transform and a smoothing. The result for the  $L = 40$ ,  $J = 200$  case, for better statistics, is displayed in Fig. 14. It clearly shows the expected reduced correlation hole, without anything particular such as going on to zero at time  $t = T_e$ , thus proving the existence of a very significant correlation between energies and intensities. Note that the energies

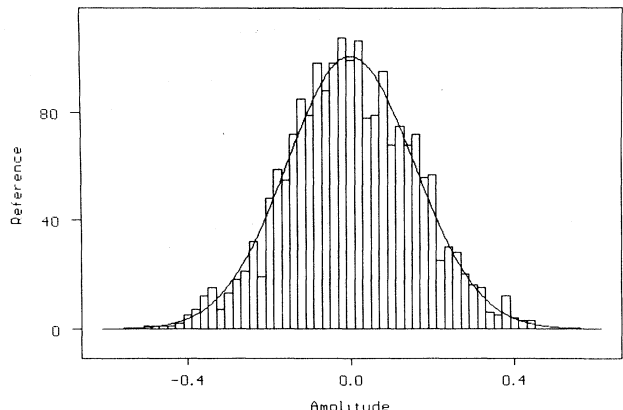


FIG. 12. Histogram of amplitudes of the chaotic spectrum  $\Lambda = L$ , symmetry  $+$ ,  $L = 40$ ,  $J = 200$ ,  $2B = 2.5 \times 10^{-12}$ ,  $K = -12.5$ ,  $\nu_{200} = 877.5 \pm 25.0$ , centered on  $T_e/T_N = 0.331$  (symmetry  $+$  levels contained in the spectrum which led to Fig. 11). The theoretical curve is a Gaussian function, as expected for a chaotic system, with no adjustable parameter: its standard deviation is  $1/\sqrt{(L+1)}$ , and its amplitude is deduced from the number of levels and the bin width (0.02). Notice that there is an ambiguity in the overall sign of the wave function [coefficient  $A_\Lambda$  of Eq. (2.7)], and that the overall signs at different energies cannot be related. We have chosen to set positive the sign of  $A_0$ . The symmetry of the curve shows the additional result that there is no sign correlation between  $A_0$  and  $A_{40}$ . Similar results are obtained for the  $-$  symmetry.

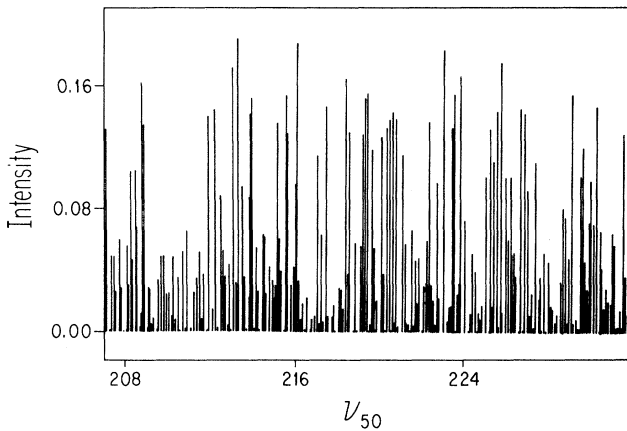


FIG. 13. Spectrum of Fig. 5, after shuffling randomly the intensities of the lines in all the energy ranges, keeping the positions of the levels. Intensity and spacings statistics are unchanged, but any correlation between them is destroyed.

did show the correlation hole perfectly in the smoothed Fourier transform in Fig. 8. The effect thus must be one of energy-amplitude correlation.

At this point a digression to nuclear physics seems in order: There the partial neutron width provides a set of intensities that satisfy the criteria put forward in [30], not for an entire basis but at least for one component and that is all we need. In this case it was always assumed that no correlation between energies and amplitudes exists and a simple test in Ref. [31] seemed to confirm this point. In this reference the deviation of the unfolded energy levels from those of a picket fence (equidistant) spectrum are correlated with the partial width, the result being zero within statistical accuracy. We performed the same test on our spectra and again obtained zero. This immediately raised the question whether nuclear data would resist the obviously more stringent test of the correlation hole in a Fourier transform. Using data from the nuclear data ensemble graciously put at our disposition by O. Bohigas we obtained the ensemble averaged and smoothed Fourier transform shown in Fig. 15(b)

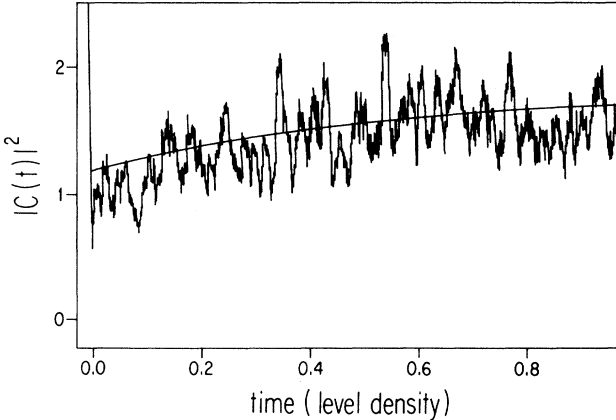


FIG. 14. Fourier transform of the spectrum which led to Fig. 11, after shuffling the intensities. The hole at time  $T_e=1$  has disappeared, indicating that it was due to intensity-spacings correlations.

for the neutron-energy spectra weighted by the neutron width. This figure is complemented for completeness by the corresponding Fourier transform of the unweighted spectrum. The figures clearly show the expected correlation holes reduced in one case, complete in the other. Thus we can conclude that the nuclear data ensemble seems to display independence of amplitudes and energy levels also under this more stringent test.

In the statistical analysis of the experiments, up to now the independence of intensities and levels has always been taken for granted to a point where we find that only one and in fact fairly weak test has ever been applied. The analysis of the Rydberg molecule spectra has not only shown that this independence is not generally true, but that Fourier transforms constitute a powerful method to detect such dependencies.

We would now like to see whether these correlations can also be displayed and detected by means nearer to those used in conventional level statistics. An improved version of the correlation used in [31] can readily be defined by correlating the deviation from average intensity for any given level with the deviation from average intensities for all levels encountered within half a mean level spacing of a given energy separation from the first level. Such a correlation measure displays strong effects for our spectra but it has the evident disadvantage that it is very sensitive to small, and therefore necessarily inexact, amplitudes.

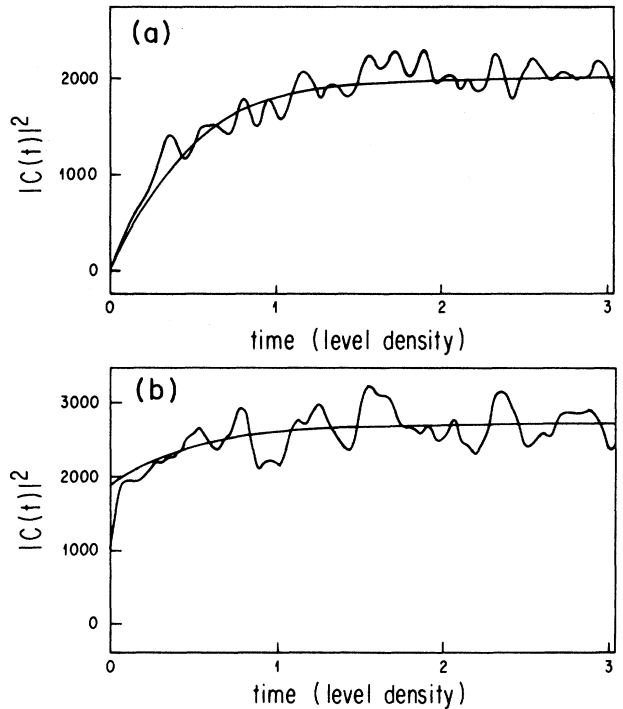


FIG. 15. Smoothed Fourier transform of the nuclear data ensemble. (a) Stick spectrum and full correlation hole; (b) neutron width-weighted spectrum and reduced correlation hole. In both cases the theoretical smooth curves contain no adjustable parameter. The nuclear data ensemble shows no indication of intensity-spacing correlations.

We thus proceed to define the intensity variance  $\sigma^2$  as

$$\sigma^2(l) = \frac{\left\langle \left( \sum_{l_0 \leq i \leq l_0 + l} I(i) - l\langle I(i) \rangle \right)^2 \right\rangle}{\langle I(i) \rangle}, \quad (5.1)$$

where the averages  $\langle I(i) \rangle$  are to be taken over the entire spectrum and the average of the sum is taken by moving  $l_0$  along the spectrum. How to take this latter average practically has no well-defined answer. Clearly if we only use contiguous intervals of length  $l$  we loose information; if, on the other hand, we move the interval only by one mean level spacing or less we compute much redundant information for large  $l$ . Leaning on experience with the usual number variance we propose to proceed to move the interval in steps of length  $l/2$ .

We display  $\sigma^2(l)$ , the intensity spectra for  $\Lambda = 20, 30$ , and  $40$ , in Fig. 16 for the short  $l$  range region and in Fig. 17 for a range of  $l$  which encompass more than two 41-level periods. The periodic features are displayed clearly but we also see that the result depends strongly on  $\Lambda$ . This again indicates the presence of energy-amplitude correlations.

It is now interesting to understand the precise relation between the Fourier transform and the intensity variance. This relation is a consequence of the fact we prove in Appendix B that the known relation [32]

$$\Sigma^2(l) = \int [1 - b_2(\tau)] l^2 \left( \frac{\sin(\pi l \tau)}{\pi l \tau} \right)^2 d\tau, \quad (5.2)$$

where  $[1 - b_2(\tau)]$  is precisely the full correlation hole obtained in Fourier transforming a stick spectrum, extends to  $\sigma^2$  and the reduced correlation hole obtained in Fourier transforming a real, intensity-weighted signal

$$\sigma^2(l) = \int |\tilde{C}(t)|^2 l^2 \left( \frac{\sin(\pi l \tau)}{\pi l \tau} \right)^2 d\tau, \quad (5.3)$$

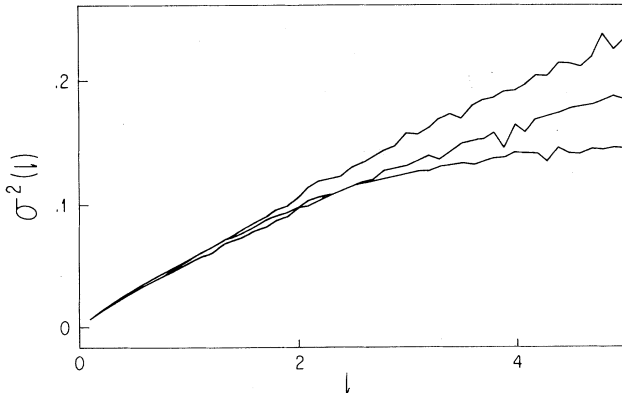


FIG. 16. Intensity variance  $\sigma^2(l)$  for small  $l$  for  $\Lambda = 20, 30, 40$  excitation (top to bottom) in the chaotic case  $L = 40$ , symmetry +,  $J = 200$ ,  $2B = 2.5 \times 10^{-12}$ ,  $K = -12.5$ ,  $\nu_{200} = 877.5 \pm 25.0$ , centered on  $T_e/T_N = 0.331$ . The fact that the curves vary with  $\Lambda$  shows that there are intensity-spacing correlations.

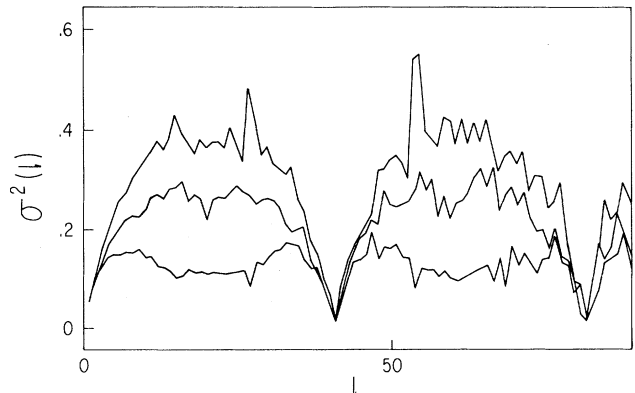


FIG. 17. Same as Fig. 16 for large  $l$ , showing the 41 periodicity due to the quasiperiodicity of the spectrum.

where  $\tilde{C}(t)$  is the Fourier transform of the spectrum minus its average (which gives the fast initial transient seen in all our FT figures). This relation is valid for a single spectrum and implies no ensemble average nor statistical hypothesis. The intensity variance is thus basically an average of  $|C(\tau)|^2$  between  $\tau = 0^+$  and  $\tau = l$ .

The two methods are thus complementary: the Fourier transform has a clearer physical meaning, when one remember that it gives the time evolution of the system, but the intensity variance has a better signal-to- (statistical) noise ratio because of this averaging, especially for short or medium  $l$  ranges. We thus found an alternative easy to use measure of chaos for intensity spectra that, like the Fourier transform, is not sensitive to small errors in the experiment or calculation. Levels that are missed entirely or whose amplitude is poorly calculated are irrelevant as long as the corresponding true and computed amplitudes are small. There is one important exception to this last point: The level density must be known correctly and thus if many levels are missed completely this density cannot be taken from the calculated or measured spectrum [9]. For practical computations of the intensity variance for small or medium  $l$  it is better to use the formula (5.1) than the in-principle equivalent formula (5.3) because, first, the computing time is much smaller, second, one avoids the problems encountered in level unfolding for large energy ranges [9].

We can now proceed to discuss our results. This will have to happen from two quite different points of view. First, we shall try to understand what we can learn about the properties of Rydberg molecules from the analysis we performed. Second, we can try to draw general conclusions about what to look for and what to expect if we intend to analyze spectra with their intensities.

## VI. CONCLUSIONS ON RYDBERG MOLECULES

We have presented a large amount of information about Rydberg molecules and actually calculated many more results of a similar nature. Now we shall try to draw conclusions from our results. First we have discerned a very strong dominance of an approximate period and its multiples in the system. We can identify this period as

the excursion period of the electron. While this is not a constant the differences between the shortest and longest orbitals that are coupled by the core interaction are only of the order of 5%. Now it is quite clear that the shortest periodic orbit must have at least this period and it is actually easy to check that several (four) isolated unstable periodic orbits with this period exist. Yet in clear distinction to other systems orbits with larger periods do not occur with a smoothly increasing density. Rather the next periodic orbits must have periods roughly two or three times as long. Only with multiples of 20 or more (see Fig. 3) the 5% spread in periods begins to be large enough to blur the bunching of periods. If we take into account the mechanism that leads to the generalized Selberg trace formulas of Gutzwiller [22] we can easily understand the frequency peaking and the near-periodic behavior of the number and intensity variances.

Recall the argument of Berry [17, 33] that determines the long-range stiffness also known as the kink [13] in  $\Delta_3$  or  $\Sigma^2$  statistics. It was based on the existence of a shortest periodic orbit that in turn was responsible for the shortest times involved. These determine the long-range correlations in energy and by consequence the lowest frequencies in the Fourier transforms of the spectra. In the present case we have the special situation that for all cases, ordered, intermediate, or chaotic, we have the same period, namely the period of the unperturbed hydrogenic orbits. Thus the position of the kink can be fixed without considering the detailed structure of the classical orbits.

Proceeding to interpret our results for amplitudes, we find a very clear correlation between amplitudes and energies. It is important to realize that this correlation goes beyond the periodic structure as noticed in the energy spectra. Remember that by simply smoothing the Fourier transform of the energies we recovered the full correlation hole [3] as expected [Fig. 8(b)]. On the other hand, to recover the reduced correlation hole on the intensity spectrum, which is expected for a Porter-Thomas distribution of the amplitudes independent of the spacings, we had to destroy explicitly the correlation between amplitudes and energies (Fig. 14).

The Fourier spectrum for an individual wave packet in Fig. 11 displays a fairly strong suppression for the time corresponding to the period of the shortest closed trajectory. This may be understood if we consider the first iteration on the Poincaré plot of the classical probability density corresponding to the wave packet we chose [Fig. 6(b)], or the Wigner function of the same [Fig. 7(b)]. Indeed for a packet concentrated near the north pole of the section ( $\Lambda = L$ ) we see that the first iterate falls into a region very remote from the initially covered area. Thus it clearly does not touch the shortest periodic orbits which correspond to an invariant point on this map. The shape of this first iterate is physically very significant and easy to understand. With  $T_e/T_N = 0.331$ , the initial ring first rotates by  $\sim 1/3$  of a turn around the  $OX$  axis, conserving its shape, then the collision with the core gives a strong  $\cos(\theta_e)$ -dependent rotation around the  $OZ$  axis, which stretches it in the direction perpendicular to this axis. The process repeats at the next iteration giv-

ing rapidly a filamentary structure which fills the sphere uniformly. This kind of "baker's transformation" leading to "mixing" is one of the essential ingredients of classical chaos. To confirm the interpretation we have done the same analysis choosing a  $L = 40$ ,  $\Lambda = 20$  packet. The FT of the spectrum (Fig. 18) shows that the first frequency has an amplitude nearer to the average rather than zero, and indeed the surface of section (not displayed here) shows the packet to have significant overlap with itself after the first iteration. For any initial wave packet after a few iterations the overlap between the initial and the time propagated packet is constant, which is precisely the definition of classical mixing.

The fact that these features are seen not only on the classical map but also for the Wigner functions underscores the fact that this interpretation carries through to quantum mechanics. The reason is readily understood when one notices the following. The Fourier transform of the spectrum is equal to the autocorrelation function of the dipole moment [34],

$$C(t) = \langle d(0)d(t) \rangle. \quad (6.1)$$

This, as we show in Appendix C, implies that its square modulus which is plotted, e.g., in Fig. 11, is equal to the autocorrelation function of the Wigner function,

$$|C(t)|^2 = \langle W(0)W(t) \rangle \\ = \int \int W(p, q, 0)W(p, q, t)dp dq, \quad (6.2)$$

i.e., just the overlap between Wigner functions at times 0 and  $t$  as displayed, e.g., in Fig. 7. The similitude between corresponding Poincaré sections and Wigner functions translate thus immediately in the preceding interpretation of quantum Fourier transforms in terms of classical periodic orbits. This shows also that, while in classical mechanics the precise definition of mixing is for infinite times, there is in quantum mechanics a practical time

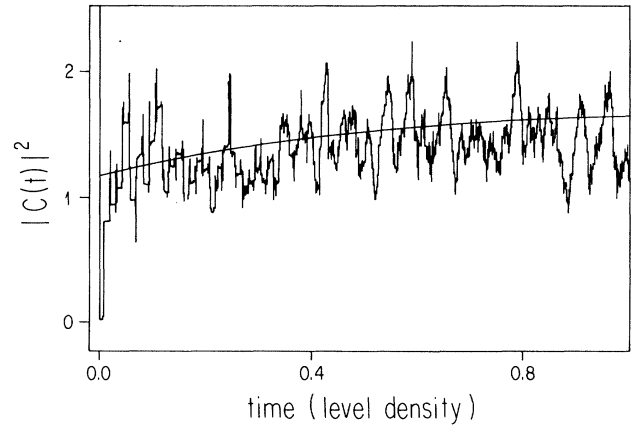


FIG. 18. Smoothed Fourier transform for an intensity-weighted spectrum for a  $\Lambda = L/2 = 20$  excitation in the same chaotic case as in Fig. 11. Here the hole at the origin is not significant, its width is  $T_e/2$ : it is due to the fact that smoothing has been made between times  $t - T_e/2$  and  $t + T_e/2$ , and that there is nothing before the time  $T_e$ . The first recurrence has the expected intensity.

limitation: the time needed for the system to mix on a length scale given by the wavelength (equal to  $1/L$  the radius of the sphere in the present case), because the Wigner function, due to the wave nature of the underlying wave function, cannot vary significantly on scales shorter than the wavelength. For longer times each successive Wigner function seems to be approximately an independent random sample on that  $1/L \times 1/L$  grid on the sphere, giving for the overlaps the "noise" of one standard deviation  $\sqrt{L}/L$  observed in Figs. 11 and 18.

Now consider a set of five wave packets chosen as follows: Take the  $\Lambda = 40$  packet and rotate it by the angles  $(\theta, \phi) : (0^\circ, 0^\circ)(45^\circ, 0^\circ)(45^\circ, 90^\circ)(90^\circ, 0^\circ)(90^\circ, 90^\circ)$ . In Fig. 19 we show the superposition of the five corresponding Fourier transforms. Note that this is quite different from the transform of an average over the five spectra. The average over all intensity spectra for a complete and orthogonal set of projections will obviously return the energy spectrum, and we saw that the correlation hole is already almost complete with a superposition of the above-mentioned five packets only. The superposition of Fourier transforms is an ensemble average of sorts over states. The result is not obvious but again we find that the 33% correlation hole is quite well established for fairly small superpositions. This implies that the correlations for different functions are essentially independent.

Finally in Fig. 20 we have displayed the sum of 41 TF corresponding to the 41 values of  $\Lambda$ . The reduced correlation hole appears now with a convincing signal-to-noise ratio, and the first channel value of one-half shows that, averaged over all possible values of  $\Lambda$ , there is a reduced overlap between Wigner functions at times zero and one basic period. This gives probably a measure, which has yet to be determined precisely, of the average of the Lyapunov exponents over the sphere, i.e., of the Kolmogorov entropy.

The intensity variances support the picture we have seen. The periodic features are quite strong but vary for different values of  $\Lambda$ . The very fact that results depend on  $\Lambda$  indicates the existence of energy-intensity correlations. We could repeat the above-mentioned superposi-

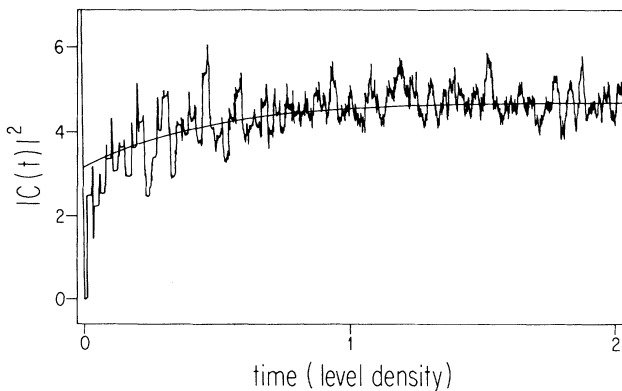


FIG. 19. Sum of the Fourier transforms of five spectra corresponding to minimum extension wave packets centered around  $(\theta_e, \phi_e) = (0^\circ, 0^\circ), (45^\circ, 0^\circ), (45^\circ, 90^\circ), (90^\circ, 0^\circ)$ , and  $(90^\circ, 90^\circ)$ , for the  $L = 40$ , symmetry +,  $J = 200$  chaotic case. We recover the reduced correlation hole.

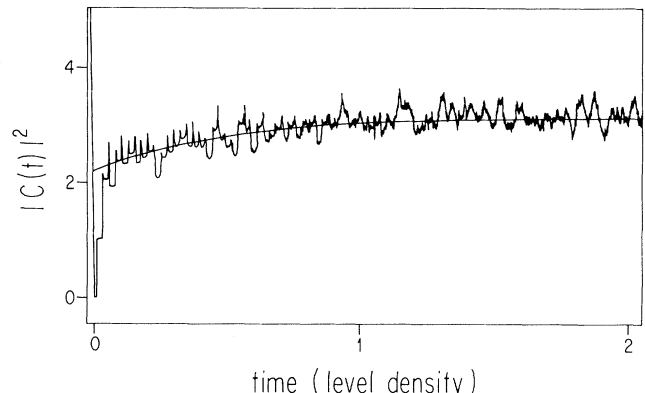


FIG. 20. Sum of the Fourier transforms of the 41 spectra corresponding to all values of  $\Lambda$  for + symmetry. We recover the reduced correlation hole, but also a significant  $\frac{1}{2}$  first channel, which corresponds to a sort of measure (to be defined more precisely) of the Kolmogorov entropy.

tions to show that we retrieve the expected GOE result, but this would only confirm what we already know from the Fourier transforms.

We may summarize that we have learned to interpret the chaotic features of Rydberg molecules. There are three ingredients in the interpretation. First, the short-term motion (for times of the order of the basic electron period) is regular and quasiharmonic, giving the regularly recurrent motion in Fourier transform and the periodic structure of the intensity variance  $\sigma^2(l)$ . Second, the global chaos, giving GOE level spacings and independent Porter-Thomas distributed line intensities, is recovered by averaging the FT spectrum over periods equal to the basic electron period, giving a full or reduced correlation hole whether or not one introduces line intensities, and it starts for times greater than the one needed to obtain mixing on a length scale given by the quantum wavelength. Third, for shorter times the nonuniversal initial state dependent transient toward mixing is contained in energy-intensity correlations.

## VII. CONCLUSIONS ON SPECTRAL STATISTICS

Maybe more important than the above-mentioned implications for spectra of Rydberg molecules are the general ideas on spectral statistics we may infer from these results. Some years ago it was noted that apparently strong harmonic components could appear for spectra of Hamiltonians that had no harmonic components [35]. In this case a clear explanation was not available. Here we have a clear physically relevant and experimentally accessible case where the nonuniversal features of the spectra are most relevant and, furthermore, quite understandable. It introduces us to the realm of statistical analysis of nonuniversal properties. This is an important and logical step along the line of research. Universal properties are of interest while their validity is tested and its domain established, but we have reached the point where GOE statistics plus long-range stiffness for a chaotic system do not surprise anyone. For integrable systems we

know that the limit where universal behavior is attained is occasionally quite far off [24]. While this happens for exotic systems like the square well it is not typical [36]. But for completely or almost completely chaotic systems this problem was not considered important and at least billiards seem to behave adequately, though recently deviations due to the bouncing-ball states in the stadium have been observed [37]. Thus for the chaotic regime this near-periodicity is to a large extent a new feature: of course it occurs normally in regular [27] or mixed [28] systems. The near-periodicity can be understood as an extension of the long-range stiffness, but the uncovered correlation between energies and intensities obliges us to take a look at other systems were we took their independence for granted.

In particular take the nuclear data ensemble. As we mentioned earlier the tests performed previously were not sensitive to the correlation discovered in Rydberg molecules. But also the test we performed is not really conclusive for the following reason. In Fig. 19 we showed that a superposition of only five Fourier spectra simulate the 33% correlation hole already quite well despite the fact that individual spectra do not do this. On the other hand, in the nuclear data ensemble we make an ensemble average over many nuclei and we certainly expect correlations in different nuclei to be independent. Thus individual nuclei will have to be tested to obtain a corresponding answer. This, on the other hand, seems difficult in view of the short spectra that are available. At this point though the other and very important new aspect of the analysis of intensity spectra enters. Most experimentally available spectra are limited by three factors: insufficient experimental resolution, omission of small intensities, and natural linewidth. All these factors will certainly destroy information on short-range correlations, but the correlation hole of the Fourier transform as well as the long-range part of the intensity variance defined in this paper are not sensitive to short-range discrepancies. Natural linewidth may still spoil our game as interferences tend to become dominant, leading in the end to Ericson fluctuations. But in this case a bound description of the system may become doubtful anyway. On the other hand, the first two problems clearly may be overcome by studying intensity spectra in the way mentioned above. Small intensities and small errors in position do not significantly alter the results as long as we know the level densities reasonably well. We thus have instruments to study intensity spectra that are not too well resolved and with some noise. This will permit us to use longer sequences in nuclear physics and many more spectra in molecules.

If several different intensity spectra of the same total system are available we can also do other kinds of analyses, starting with a simple superposition of spectra to obtain results that may display the universal features more closely.

Summarizing we may say that the analysis of intensity spectra by means of the Fourier transform and intensity variances as well as eventually by the generalizations of  $\Sigma^3$  and  $\Sigma^4$  or the reduced quantities  $\gamma_1$  and  $\gamma_2$  often used to investigate properties of the three- and four-point

correlation function [38] opens a new domain for analysis and access to understanding of features that were not previously amenable to analysis by spectral statistics.

## ACKNOWLEDGMENTS

We are greatly indebted to P. Labastie for numerous bits of advice about the MQDT method and numerical difficulties it involves, to A. Pandey for pointing out previous work on intensity-level correlations [31], and to O. Bohigas for kindly communicating the nuclear data ensemble.

## APPENDIX A: THE REDUCED CORRELATION HOLE

Due to its importance in the present paper, we give here the proof of this result which was announced without proof in Ref. [3] (which contained a misprint).

The Fourier transform of the absorption spectrum

$$S(\omega) = \sum_e |\langle g|d|e\rangle|^2 \delta(\omega - (E_e - E_g)), \quad (A1)$$

where we have supposed a single ground state, is equal to

$$C(t) = \sum_e |\langle g|d|e\rangle|^2 \exp[-i(E_e - E_g)t] \quad (A2)$$

so that

$$|C(t)|^2 = \sum_{e,e'} I_e I_{e'} \exp[-i(E_e - E_{e'})t], \quad (A3)$$

where we have put  $I_e = |\langle g|d|e\rangle|^2$ , depends only on the Bohr frequencies of the excited state, not on the energy of the single ground state.

This formula is exact for a single spectrum. Statistical theory of spectra consist in averaging this formula over an ensemble of spectra. Typically this ensemble average is replaced by an energy average over a long enough spectrum. The consequence of this procedure is that the theoretical formula for an ensemble of spectra gives smooth results, whereas the actual Fourier transform of a single spectrum has a very noisy "speckle" structure [3], which we have found in the present work and discussed in Sec. III. These speckle structures contain information about the individual line positions, which is lost by averaging over an ensemble. Conversely, the accuracy of the reconstruction of the statistical properties by smoothing a single spectrum over the speckles structure is limited by the number of levels contained in this spectrum. The speckle structure itself has statistical properties consistent with this obvious limitation [9].

We then separate terms where  $e = e'$  and terms where  $e \neq e'$  and replace the discrete sums in Eq. (A3) by probability averages

$$|C(t)|^2 = \int \int I_e^2 P(I_e, E_e) dI_e dE_e + \int \int \int I_e I_{e'} \exp[-i(E_e - E_{e'} t)] P(I_e, I_{e'}, E_e, E_{e'}) dI_e dI_{e'} dE_e dE_{e'}. \quad (\text{A4})$$

We then suppose independence of the level spacings and intensities so that the probabilities split into products, in particular

$$P(I_e, I_{e'}, E_e, E_{e'}) = P(I_e)P(I_{e'})[R_1(E_e)R_1(E_{e'}) - T_2(E_e, E_{e'})] \quad (\text{A5})$$

with the notations and normalizations of Mehta [39] for the level density  $R_1$  and the two-point correlation  $T_2$ . Taking reduced energy units  $n = E_e/R_1(E_e)$  and a reduced time  $\tau = R_1 t$  (which supposes that  $R_1$  is constant, i.e., that the spectrum has been unfolded), leads to

$$|C(t)|^2 = N\langle I^2 \rangle + \langle I \rangle^2 \int \int_{-N/2}^{+N/2} \exp[-i(n - n')\tau][1 - Y_2(n - n')]dn dn', \quad (\text{A6})$$

where  $Y_2$  is the Dyson's two-point cluster function and  $N$  the total number of levels in the spectrum. Changing the variables of integration to  $y = n + n'$  and  $x = n - n'$  in the  $Y_2$  term leads this part of the integral to be equal to

$$\int_{-N}^{+N} \exp(-ix\tau) Y_2(x)(N - |x|)dx. \quad (\text{A7})$$

In the usual case where  $N \gg 1$ , the  $N - |x|$  term is equal to  $N$  in the range of  $x$  of order unity in which  $Y_2$  is non-negligible, so that this integral reduces to  $N$  times the two-level form factor  $b_2(\tau)$ , the Fourier transform of  $Y_2$ . Finally,

$$|C(t)|^2 = N^2\langle I \rangle^2[\sin(N\tau)/(N\tau)]^2 + N\langle I^2 \rangle - N\langle I \rangle^2 b_2(\tau). \quad (\text{A8})$$

The  $N^2$ -dependent term gives the fast initial transient seen in all our figures of Fourier transforms. For stick spectra, when  $\langle I \rangle^2 = \langle I^2 \rangle = 1$  the remaining terms are equal to  $N[1 - b_2(\tau)]$ , which gives the correlation hole. It is 100% deep, i.e., FT goes to zero if  $b_2$  corresponds to GOE statistics. If one takes into account the intensities it is reduced by a factor  $\langle I \rangle^2/\langle I^2 \rangle = 1/3$  for Porter-Thomas statistics [40].

## APPENDIX B: INTENSITY VARIANCE AND FOURIER TRANSFORM

We start from the relation [see Eq. (5.1) and comments that follows]

$$S_l = \left\langle \left( \sum_{l_0 \leq E_i \leq l_0 + l} I(i) \right)^2 \right\rangle = \int \left( \int S(E) W_l(E - l_0) dE \right)^2 dl_0, \quad (\text{B1})$$

where  $W_l(E - l_0) = H(E - l_0) - H(E - (l_0 + l))$  is a window function of width  $l$  starting at  $l_0$  ( $H$  is the Heaviside step function), and  $S(E)$  is the spectrum. The inner integral is a function of  $l_0$  which is a convolution integral that becomes a simple product by Fourier transform. Writing

it as the inverse Fourier transform of its Fourier transform leads to

$$S_l = \int \int e^{il_0\tau} C(\tau) \hat{W}_l(\tau) d\tau \times \int e^{il_0\tau'} C(\tau') \hat{W}_l(\tau') d\tau' dl_0, \quad (\text{B2})$$

where  $C(\tau)$  is the Fourier transform of the spectrum and  $\hat{W}_l(\tau)$  the Fourier transform of the window function. Integrating first on  $l_0$  gives a  $\delta(\tau + \tau')$ , and taking into account that for the Fourier transform of a real function a change of sign of  $\tau$  is equivalent to complex conjugation leads, introducing the known value of  $\hat{W}(\tau)$ , to the final result

$$S_l = \int |C(\tau)|^2 l^2 \left( \frac{\sin(\pi l\tau)}{\pi l\tau} \right)^2 d\tau. \quad (\text{B3})$$

The  $\langle I(i) \rangle$  remaining term in Eq. (5.1) cancels the fast component at the origin of the Fourier transform [see Eq. (A8)], which stays there because one does not usually subtract the average of the spectrum before Fourier transforming it. Thus this relation is valid for a single spectrum, independent of ensemble averaging, and this proof settles the problem of the choice of the step in  $l_0$ , which is in principle very small. The choice of a step of  $l/2$  we have made is a reasonable compromise with respect to computing time.

## APPENDIX C: FOURIER TRANSFORM AS OVERLAP OF WIGNER FUNCTIONS

We start from the well-known fact [34] that the Fourier transform (A2) of the spectrum (A1) can be rewritten as

$$C(t) = \sum_e \langle g | d | e \rangle [\exp(-iE_e t) \langle e | d | g \rangle \exp(iE_g t)] = \text{Tr}[d(0)d(t)] = \int [\psi(q, 0)]^* \psi(q, t) dq, \quad (\text{C1})$$

where  $\psi(q, 0) = d|g\rangle$  is the image of the ground state  $|g\rangle$  on the excited electronic state by the dipole operator  $d$ . Then

$$\langle W(p, q, 0)W(p, q, t) \rangle = \int \int \int \psi(q - r, 0) \exp(2ipr) \psi^*(q + r, 0) dr \int \psi(q - r', t) \exp(2ipr') \psi^*(q + r', t) dr' dp dq.$$

(C2)

Inverting the order of integrals, the integral over  $p$  gives a  $\delta(r + r')$ , then one takes as integral variables  $q_1 = q - r$  and  $q_2 = q + r$ , leading to the desired result

$$\begin{aligned} \langle W(p, q, 0)W(p, q, t) \rangle &= \int \int \psi(q_1, 0) \psi^*(q_2, 0) \psi(q_2, t) \psi^*(q_1, t) dq_1 dq_2 \\ &= \left| \int \psi^*(q, 0) \psi(q, t) dq \right|^2 \\ &= |C(t)|^2, \end{aligned}$$

(C3)

according to Eq. (C1).

- \* Permanent address: Instituto de Física, Universidad Nacional Autónoma de México, Apartado Postal 139-B, 62191 Cuernavaca Morelos, Mexico.
- [1] D.W. Noid, M.L. Koszykowksi, and R. Marcus, *Annu. Rev. Phys. Chem.* **32**, 267 (1981); E.J. Heller and R.L. Sundberg, *Proceedings of the NATO Advanced Research Workshop on Chaotic Behavior in Quantum Systems*, edited by G. Casati (Plenum, New York, 1985), p. 255.
  - [2] E. Abramson, R.W. Field, D. Imre, and J.L. Kinsey, *J. Chem. Phys.* **80**, 2298 (1986).
  - [3] L. Leviandier, M. Lombardi, R. Jost, and J.P. Pique, *Phys. Rev. Lett.* **56**, 2449 (1986); R. Jost and M. Lombardi, *Quantum Chaos and Statistical Nuclear Physics*, edited by T.H. Seligman and H. Nishioka, Lecture Notes in Physics Vol. 263 (Springer, Heidelberg, 1986), p. 72; M. Lombardi, J.P. Pique, P. Labastie, M. Broyer, and T.H. Seligman, *Comments At. Mol. Phys.* **25**, 345 (1991).
  - [4] J.P. Pique, Y. Chen, R.W. Field, and J.L. Kinsey, *Phys. Rev. Lett.* **58**, 475 (1987).
  - [5] M. Lombardi, P. Labastie, M.C. Bordas, and M. Broyer, *J. Chem. Phys.* **89**, 3479 (1988).
  - [6] M. Broyer, G. Delacrétaz, G.Q. Ni, R.L. Whetten, J.P. Wolf, and L. Wöste, *Phys. Rev. Lett.* **62**, 2100 (1989); J.M. Gomez-Llorente, H.S. Taylor, and E. Polak, *ibid.* **62**, 2096 (1989).
  - [7] T. Guhr and H.A. Weidenmüller, *Chem. Phys.* **146**, 21 (1990); U. Hartmann, H.A. Weidenmüller, and T. Guhr, *ibid.* **150**, 311 (1991).
  - [8] W.F. Polik, D.R. Guyer, W.H. Miller, and C.B. Moore, *J. Chem. Phys.* **92**, 3471 (1990).
  - [9] A. Delon, R. Jost, and M. Lombardi, *J. Chem. Phys.* **95**, 5701 (1991).
  - [10] D. Wintgen and H. Friedrich, *Phys. Rev. Lett.* **57**, 571 (1986); D. Delande and J.C. Gay, *ibid.* **57**, 2006 (1986); A. Holle, J. Main, G. Weisbuch, H. Rottke, and K.H. Welge, *Phys. Rev. Lett.* **61**, 161 (1988). For more recent reviews see *Comments At. Mol. Phys.* **25** (1990).
  - [11] O. Bohigas, M.J. Giannoni, and C. Schmit, *Phys. Rev. Lett.* **52**, 1 (1984).
  - [12] O. Bohigas, M.J. Giannoni, C. Schmit, S. Tomsovic, and D. Ullmo, *Comments At. Mol. Phys.* **25**, 31 (1990).
  - [13] T.H. Seligman, J.J.M. Verbaarschot, and M. Zirnbauer *Phys. Rev. Lett.* **53**, 215 (1984); *J. Phys. A* **18**, 2751 (1985).
  - [14] O. Bohigas, S. Tomsovic, and D. Ullmo, *Phys. Rev. Lett.* **64**, 1479 (1990); **65**, 5 (1990).
  - [15] P. Labastie, M.C. Bordas, B. Tribollet, and M. Broyer, *Phys. Rev. Lett.* **52**, 1681 (1984); M.C. Bordas, M. Broyer, J. Chevaleyre, P. Labastie, and S. Martin, *J. Phys.* **46**, 27 (1987).
  - [16] T.A. Brody, J. Flores, J.B. French, P.A. Mello, A. Pandey, and S.S.M. Wong, *Rev. Mod. Phys.* **53**, 385 (1981).
  - [17] M.V. Berry, *Proc. R. Soc. London Ser. A* **400**, 229 (1985).
  - [18] G. Herzberg, *Molecular Spectra and Molecular Structure. I Spectra of Diatomic Molecules*, 2nd ed. (Van Nostrand Reinhold, New York, 1950).
  - [19] K. Nakamura, Y. Okazaki, and A.R. Bishop, *Phys. Rev. Lett.* **57**, 5 (1986).
  - [20] U. Fano, *Phys. Rev. A* **2**, 253 (1970); *J. Opt. Soc. Am.* **65**, 979 (1975); C. H. Greene and C. Jung, *Adv. At. Mol. Phys.* **21**, 51 (1985).
  - [21] A. Messiah, *Mecanique Quantique* (Dunod, Paris, 1962).
  - [22] M.C. Gutzwiller, *Chaos in Classical and Quantum Mechanics* (Springer, Heidelberg, 1990).
  - [23] B. Lesche and T.H. Seligman *J. Phys. A* **19**, 94 (1986).
  - [24] G. Casati, B.V. Chirikov, and I. Guarneri, *Phys. Rev. Lett.* **54**, 1350 (1985); M. Feingold, *Phys. Rev. Lett.* **55**, 2626 (1985).
  - [25] M.V. Berry, *Nonlinearity* **1**, 309 (1988).
  - [26] J.J.M. Verbaarschot, *J. Phys. A* **20**, 5589 (1987).
  - [27] G.R. Welch, M.M. Kash, C. Iu, L. Hsu, and D. Kleppner, *Phys. Rev. Lett.* **62**, 893 (1989).
  - [28] A. Hönig and D. Wintgen, *Phys. Rev. A* **39**, 5642 (1989).
  - [29] C.E. Porter and R.G. Thomas, *Phys. Rev.* **104**, 483 (1955).
  - [30] F. Leyvraz, J. Quezada, and T.H. Seligman, in *Proceedings of the International Colloquium on Group Theoretical Methods in Physics*, edited by V. Yodenov and W. Manke, Lecture Notes in Physics Vol. 382 (Springer, Heidelberg, 1991), p. 418; F. Leyvraz, J. Quezada, T.H. Seligman, and M. Lombardi, *Phys. Rev. Lett.* **67**, 2921 (1991).
  - [31] O. Bohigas, R.U. Haq, and A. Pandey, *Nuclear Data for Science and Technology*, edited by K.H. Boeckhoff (Reidel, Dordrecht, 1983), p 809.
  - [32] F.J. Dyson and M.L. Mehta, *J. Math. Phys.* **4**, 701 (1963).
  - [33] T.H. Seligman and J.J.M. Verbaarschot, *J. Phys. A* **18**, 2227 (1985).
  - [34] M. Baranzer, *Atomic and Molecular Processes*, edited by D. R. Bates (Academic, New York, 1962), p. 493.

- [35] T.H. Seligman, J.J.M. Verbaarschot, and H.A. Weidenmüller, Phys. Lett. B **167**, 86 (1986).
- [36] T.H. Seligman and J.J.M. Verbaarschot, Phys. Rev. Lett. **56**, 2767 (1986).
- [37] U. Smilansky and H. Weidenmüller (private communication).
- [38] O. Bohigas, M.J. Giannoni, and C. Schmit, J. Phys. Lett. **45**, L1015 (1984); O. Bohigas, R.U. Haq, and A. Pandey, Phys. Rev. Lett. **54**, 1645 (1985); C.E. Roman, T.H. Seligman, and J.J.M. Verbaarschot, *Quantum Chaos and Statistical Nuclear Physics*, edited by T.H. Seligman and H. Nishioka, Lecture Notes in Physics Vol. 263 (Springer, Heidelberg, 1986), p. 72.
- [39] M.L. Mehta, *Random Matrices and Statistical Theories of Levels* (Academic, New York, 1967).
- [40] N. Ullah and C.E. Porter, Phys. Lett. **6**, 30 (1963).